Biophysical Journal, Volume 99

Supporting Material

Control of Ca^{2+} release by action potential configuration in normal and failing murine cardiomyocytes

William E. Louch, Johan Hake, Guro Five Jølle, Halvor K. Mørk, Ivar Sjaastad, Glenn T. Lines, and Ole M. Sejersted

Supplemental methods and data

A) Measurement of transient outward current (I_{TO})

I_{TO} was recorded under Na^+- and Ca^{2+}-free conditions with a pipette solution containing (in mM): 110 K-aspartate, 20 KCl, 0.5 $MgCl_2$, 4 MgATP, 5 EGTA, 5 HEPES, and 10 glucose (pH 7.2), and an extracellular solution containing (in mM): 140 cholineCl, 1.0 $CdCl_2$, 0.5 $MgCl_2$, 5.0 HEPES, 5.5 glucose, and 5.4 KCl (pH 7.4). I_{TO} was elicited by 300 ms voltage steps from -70 mV to a range of potentials (-40 to 60 mV) in 10 mV increments. Peak I_{TO} was measured as the maximal outward current relative to steady state.

B) Numerical methods for calculation of electro diffusion

The electric field that drives the advection comes from the negatively charged phospholipid head-groups in the lipid bi-layer of the sarcolemma (1, 2). The charges cause an electric double layer in close proximity to the cell membrane (3, 4). The double layer is thin as the negative potential is screened by the ions in the solution. In the double layer the potential attracts cations causing an elevated concentration of these near the membrane, while repelling anions. The charged head-groups of the membrane also serve as cation binding sites, and thus act as buffers for these ions (5, 6). It has been shown that the Gouy-Chapman theory, together with appropriate membrane association constants for the sarcolemmal buffers, can be used to resolve the electric potential in the double layer (3, 5, 7). The electric potential, Φ, is described in dimensionless units as $\Phi = \Psi/\Psi_T$, where the unit of Ψ and Ψ_T is Voltage. Ψ_T is a temperature-dependent characteristic potential given by:

$$\Psi_T = \frac{k_B T}{e}. \qquad (1)$$

A single exponential can be used to approximate Φ (7):

$$\Phi = \Phi_0 e^{-x_2/\lambda_D}. \qquad (2)$$

Here Φ_0 is the potential at the membrane, where x_2 is zero. λ_D is the Debye length, which is calculated

to be ~ 1 nm (7). Given the potential we can now state the advection-diffusion equation that governs the movement of ions in the dyad:

$$\frac{\partial c}{\partial t} = D\left[\nabla^2 c + \nabla\left(cz\nabla\Phi\right)\right]. \tag{3}$$

Here D and z are the diffusion constant and the valence of Ca^{2+}.

C) Numerical methods for the continuous model

We used a finite element method for the spatial discretization of the PDEs, and a backward Euler method for the temporal discretization. The size of the time step was determined by an adaptive time-stepping scheme based on the mean value of the relative time derivative of the included field. The advection term in Eq. 3 causes numerical problems when discretized using finite element method (8). To avoid these difficulties we transformed Eq. 3 into:

$$a\frac{\partial u}{\partial t} = D\nabla a\nabla u, \tag{4}$$

where $a = e^{-z\Phi}$, and $u = e^{z\Phi}c$, as previous studies also have done (9). The original Ca^{2+} can be retrieved by: $c = e^{-z\Phi}u$. This technique allowed us to use a coarser mesh close to the T-tubule, and the resulting linear system needed to solve each time step became symmetric. The sparse linear system was assembled using PyDOLFIN from the FEniCS project, (http://www.fenics.org), and solved using a Krylov solver from the PETSc linear algebra library(10) together with an algebraic multi-grid preconditioner from the Hypre library (11).

D) Numerical methods for the discrete models

Some of the propensity (rate) functions in the Markov models depend on the continuous variables: Ca^{2+} and V. The α and β functions depend on the membrane potential, and the activation function of the RyRs depends on the local [Ca^{2+}]. To be able to correctly evolve the stochastic system

we therefore needed to solve the discrete system coupled to these continuous variables. We developed a modified Gillespie method (12) to accomplish this.

Let $S = S(t)$ be a vector holding the present states of the included Markov models and let $N = N(S)$ be the number of possible transitions that can be undertaken from these combination of states. The propensity function of the i^{th} transition is denoted by $\lambda_i = \lambda_i(t)$. The total propensity for the next transition, $\lambda = \lambda(S, t)$, is given by a sum over all λ_i:

$$\lambda = \sum_{i}^{N} \lambda_i . \tag{S1}$$

The time for the next stochastic transition is exponentially distributed, if we assume that λ is constant. The time to the next stochastic transition, Δt_t, is realized by drawing one random number, r_1, from a uniform distribution on the unit interval and transform it according to:

$$\Delta t_t = \frac{-\ln(r_1)}{\lambda}. \tag{S2}$$

The transition time is relative to the present time in the simulation. If a transition takes place at time $t + \Delta t_t$, we need to realize which of the N possible transitions that actually took place. Drawing another random number, r_2, from the same distribution as above, does this. The k^{th} transition takes place if,

$$\sum_{j=0}^{k-1} \lambda_j \le \lambda \cdot r_2 < \sum_{j=0}^{k} \lambda_j \tag{S3}$$

where $\lambda_0 = 0$, and $k = [1 \ldots N]$. The Gillespie method assumes constant propensity functions between the transitions. However most of the included propensity functions in the LCC and RyR models are not constant, and we therefore have to modify the method. Instead of realizing a transition based on a given propensity, we realize a dimensionless time to the next transition, Δt_t^*, using $\lambda = 1$ in Eq. S2. Δt_t^* relates to the actual transition time by,

$$\Delta t_t = \frac{\Delta t_t^*}{\lambda} \tag{S4}$$

A time step, $\Delta t < \Delta t_t$, is chosen during which constant external variables is assumed, and hence constant propensity functions. To minimize the error of assuming constant continuous variables during a time step we need to choose a small Δt when such variables change greatly, for example during an upstroke of the AP. Using the chosen Δt we update the continuous system and reduce the dimensionless transition time according to,

$$\Delta t_t = \frac{-\ln(r_1)}{\lambda}. \qquad \text{(S5)}$$

Whenever Δt_t , from Eq. S4, is smaller than the chosen Δt a transition occurs before the time step is completed. We realize the transition and check whether the transition changes the status of a channel. If it does, we say that the transition is a channel transition. The continuous system is solved up to the transition time by setting $\Delta t = \Delta t_t$. Finally we realize the transition, changing the state of the continuous system. We then draw a new dimensionless transition time, Δt^* and start over again. If the transition was not a channel transition we can skip it, but we need to draw a new dimensionless transition time.

Supplemental Figure Legends

Supplemental Figure 1. 3-dimenionsal computation model of the dyad. **A.** The dyadic cleft was modeled as a cylindrical disk, with height = 12 nm. **B.** RyRs were positioned in a highly regular 2-dimensional lattice, with a 5:1 ratio between the number of RyRs and LCCs (white circles). Two dyad sizes were modeled; a large dyad (100 RyRs, 20 LCCs) and a smaller dyad (25 RyRs, 5 LCCs) **C.** LCCs were raised 2 nm from the t-tubule membrane.

Supplemental Figure 2. Markov models were employed to describe the channel dynamics of LCCs and RyRs. **A.** The 12-state LCC model initially described by Jafri et al (13) was slightly modified in our study. **B.** A minimalistic Markov model was employed for RyRs.

Supplemental Figure 3. Current-voltage relationships for transient outward current (I_{TO}). I_{TO} density was reduced in CHF myocytes across a range of voltages. n_{cells}: SHAM = 12, CHF = 10; $P<0.05$ vs SHAM.

References

1. McLaughlin SG, Szabo G, Eisenman G. 1971. Divalent ions and the surface potential of charged phospholipid membranes. J Gen Physiol. 58:667-687.

2. Langner M, Cafiso D, Marcelja S, McLaughlin S. 1990. Electrostatics of phosphoinositide bilayer membranes. Theoretical and experimental results. Biophys J. 57:335-349.

3. Grahame DC. The electrical double layer and the theory of electrocapillarity.1947. Chem Rev. 41:441-501.

4. Andelman D. Electrostatic properties of membranes: the Poisson-Boltzmann theory. In: Lipowsky R, Sackmann E, eds. Structure and Dynamics of Membranes; Handbook of Biological Physics: North-Holland, 1995:603-642.

5. Bers DM, Philipson KD, Peskoff A. 1985. Calcium at the surface of cardiac plasma membrane vesicles: cation binding, surface charge screening, and Na-Ca exchange. J Membr Biol. 85:251-261.

6. Post JA, Langer GA. 1992. Sarcolemmal calcium binding sites in heart: I. Molecular origin in "gas-dissected" sarcolemma. J Membr Biol. 129:49-57.

7. Soeller C, Cannell MB. 1997. Numerical simulation of local calcium movements during L-type calcium channel gating in the cardiac diad. Biophys J. 73:97-111.

8. Brooks AN, Hughes TJR. 1982. Streamline Upwind Petrov-Galerkin Formulations for Convection Dominated Flows with Particular Emphasis on the Incompressible Navier-Stokes Equations. Computer Methods in Applied Mechanics and Engineering. 32:199-259.

9. Cheng YH, Suen JK, Zhang DQ, Bond SD, Zhang YJ, Song YH, et al. 2007. Finite element analysis of the time-dependent Smoluchowski equation for acetylcholinesterase reaction rate calculations. Biophys J. 92:3397-3406.

10. Balay S, Buschelman K, Eijkhout V, Gropp WD, Kaushik D, Knepley MG, et al. 2006. PETSc Users Manual. Argonne National Laboratory.

11. Falgout RD, Yang UM. hypre : A Library of High Performance Preconditioners. In: 2331 ed. Berlin / Heidelberg: Springer, 2002:632-641.

12. Gillespie JH. 1977. Multilocus Behavior in Random Environments. II. Linkage Disequilibrium in an Additive Model. Genetics. 87:569-579.

13. Jafri MS, Rice JJ, Winslow RL. 1998. Cardiac Ca^{2+} dynamics: the roles of ryanodine receptor adaptation and sarcoplasmic reticulum load. Biophys J. 74:1149-1168.

Supplemental Figure 1

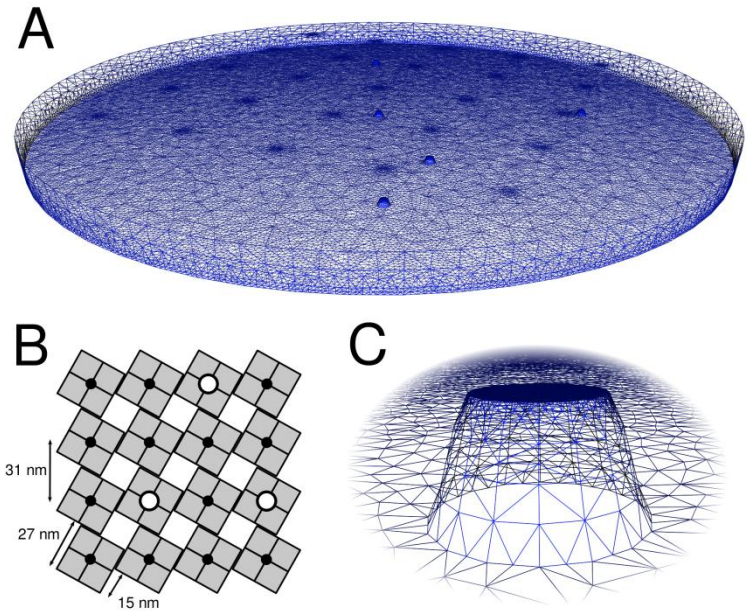

Supplemental Figure 2

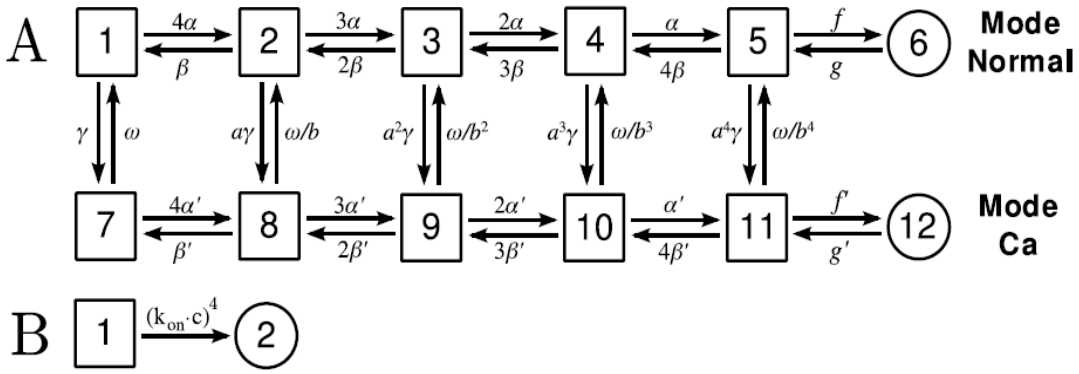

Supplemental Figure 3